Eur. Phys. J. D **2**, 279–289 (1998)

THE EUROPEAN PHYSICAL JOURNAL D

Atomic beam deflection by coherent momentum transfer and the dependence on weak magnetic fields

H. Theuer and K. Bergmann[a]

Fachbereich Physik der Universität, Erwin-Schrödinger-Str., 67663 Kaiserslautern, Germany

Received: 1 October 1997 / Revised: 22 December 1997 / Accepted: 11 March 1998

Abstract. The deflection of Ne atoms in the metastable state $^3P_2$ by coherent transfer of the momenta of 4 or 8 photons is demonstrated, based on the technique developed for coherent population transfer with delayed pulses (STIRAP). After deflection the intensity profile of the isotope of mass 20 is fully seperated from that for the undeflected atoms of mass 22. It is furthermore shown, how the interplay of Larmor precession of the electronic magnetic moment and the sequential deflection in two spatially separated zones can be used to measure the magnetic field, integrated over the flight-path between the transfer zones.

PACS. 32.80.Lg Mechanical effects of light on atoms, molecules, and ions – 32.80.Wr Other multiphoton processes – 42.65.Dv Stimulated Raman scattering; CARS

1 Introduction

The technique of coherent population transfer by STImulated Raman scattering involving Adiabatic Passage (STIRAP) induced by delayed interaction of an atom or molecule with two laser pulses, first suggested by Oreg *et al.* [1], has been developed recently [2–5]. The objective of STIRAP is to transfer all the population from a quantum state $|1\rangle$ to a quantum state $|3\rangle$. This is done by a Raman-type coupling of these states by two radiation fields, those of a pump laser and a Stokes laser, which couple the initial and final state, respectively, to an intermediate level $|2\rangle$.

The success of STIRAP relies on the fact that the Stokes laser, which couples two states that are initially not populated, interacts with the system before the interaction with the pump laser begins, and that there is a suitable overlap in time between these two pulses. In essence, the Stokes laser creates a coherent superposition of the two unpopulated eigenstates of the atomic or molecular system such that the pump laser is prevented from exciting systems from the populated state $|1\rangle$ to the intermediate level [6]. A trapped state is formed [7–9] which provides a pathway for smooth transfer of all of the population in state $|1\rangle$ to state $|3\rangle$ without ever populating the intermediate level $|2\rangle$. This latter fact is crucial to the success of STIRAP because it eliminates the dissipative process of spontaneous emission to levels other than state $|3\rangle$, which may also be coupled to the intermediate level $|2\rangle$ by dipole transitions. A condition for the adiabatic evolution involving the trapped state is that the pulse area of the laser pulse is large compared to unity, $\Omega\Delta\tau \gg 1$, where $\Delta\tau$ is the pulse length and Ω is the Rabi frequency of the respective transition, determined by the transition dipole moment μ_e and the electric field of the radiation, $\Omega = \mu_e E/\hbar$ [10]. In reality the explicit time dependence of the interaction (and thus the Hamiltonian) results in some nonadiabatic coupling during the transfer process and some population will transiently reside in the intermediate level from where it may be lost by spontaneous emission. It has been experimentally verified that this loss can be as small as 0.5% [11].

The remarkable properties of the STIRAP process have stimulated a large variety of applications in areas such as molecular reaction dynamics [12], electron collisions [13], spectroscopy [14,15], laser cooling [16], manipulation of atoms in a magneto optic trap [17] or emerging from it [18] and in the context of atom interferometry [19–21]. Future applications in other areas, such as cavity quantum electrodynamics [22] are likely to emerge soon.

In this work, we demonstrate the potential of the method for coherent momentum transfer, by showing the deflection of an atomic Ne* beam while the quantum state of the atom is preserved. For other recent work using stimulated light forces to manipulate the transversal or longitudinal velocity of atoms, see *e.g.* references [23–25]. In our case the deflected beam is fully separated from the undeflected one and thus the two isotopes of Ne of mass 20 and 22 are separated. Some earlier work along those lines was reported by Lawall *et al.* [26]. We also show, how the interplay of coherent momentum transfer in two separated transfer zones and the Larmor precession can be used for the detection of a weak magnetic field along the flight-path of the atoms.

[a] e-mail: bergmann@rhrk.uni-kl.de

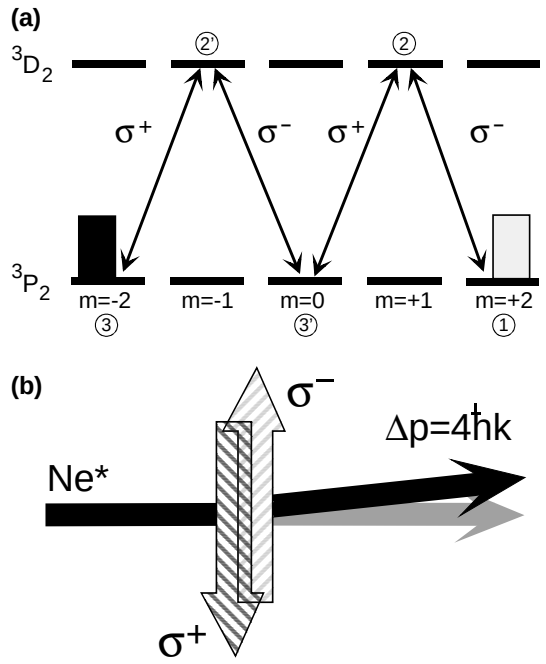

Fig. 1. (a) Levels and coupling scheme for coherent population and momentum transfer between m-substates in the $^3P_2(2p^5 3s)$ electronic state of Ne. (b) Schematic diagram of atomic beam deflection *via* coherent population transfer as shown in Figure (a). The resonant wavelength of the $^3D_2 \leftrightarrow {}^3P_2$ transition is $\lambda = 633$ nm.

2 Coherent momentum transfer

In the following, we discuss the coherent population and momentum transfer within the $^3P_2$ magnetic substates induced by circularly polarized radiation, the frequency of which is tuned to resonance with the $^3D_2$ level of the $2p^5 3p$ configuration. As shown in Figure 1 two σ^+ photons and two σ^- photons couple the $m = +2$ and the $m = -2$ state. The coupling consists of two sequential three level systems, linked by the $m = 0$ substate of the $^3P_2$ level. Population transfer in multi level and multi photon ladder systems has been considered theoretically previously [27]. Coherent transfer of population or momentum among m-substates has also been experimentally demonstrated by Pillet *et al.* [28] and Chu and coworkers [29], respectively. Nevertheless, it is instructive to briefly consider necessary conditions for the successful completion of the STIRAP process for the level scheme and linkage shown in Figure 1.

A requirement is the existence of a trapped state (a state with a zero energy eigenvalue throughout the interaction [30]). The Hamiltonian for the five level system of Figure 1 reads

$$H(t) = \frac{\hbar}{2}\begin{pmatrix} 0 & \Omega_{12} & 0 & 0 & 0 \\ \Omega_{21} & 2\Delta_{12} & \Omega_{23'} & 0 & 0 \\ 0 & \Omega_{3'2} & 2\Delta_{13'} & \Omega_{3'2'} & 0 \\ 0 & 0 & \Omega_{2'3'} & 2\Delta_{12'} & \Omega_{2'3} \\ 0 & 0 & 0 & \Omega_{32'} & 2\Delta_{13} \end{pmatrix} \qquad (2.1)$$

where Δ_{ik} is the detuning of the laser frequency from the transition frequency between levels $|i\rangle$ and $|k\rangle$. A solution of the Eigenvalue equation

$$H(t)\ \mathbf{C} = \omega\ \mathbf{C} = 0 \qquad (2.2)$$

exists if the determinant of $\hat{H}$ vanishes at all times

$$det\, H(t) = 0. \qquad (2.3)$$

Equation (2.3) can be rewritten in the form

$$det\, H(t) = 2\Delta_{13}\, det\, H_4(t) - \Omega^2_{2'3}\, det\, H_3(t) \qquad (2.4)$$

where $H_k(t)$ describes the upper left $k \times k$ submatrix of $H(t)$.

Inspection of equation (2.4) allows the identification of the condition for the formation of a state with zero energy eigenvalue. The second determinant $det\, \hat{H}_3$ relates to the three level system ($m = -2$, $m = 0$ and $m = -1$ in the $^3P_2$ and $^3D_2$ level, respectively). It is known that a zero energy eigenvalue exists, if the laser frequencies are in two photon resonance with the $m = +2$ and $m = 0$ state $\Delta_{13'} = 0$ [31]. The first determinant $det\, \hat{H}_4$ need not be evaluated, provided the four-photon resonance is also established. If $\Delta_{13} = 0$ an eigenstate $\mathbf{C}$ with zero eigenvalue exists and an adiabatic transfer path is available [5]. Since the photons of different polarization are derived from the same laser beam, maintenance of the multiphoton resonances is guaranteed provided the laser beams cross the atomic beam at right angle to eliminate any Doppler shifts. Deviation from the right angle by more than 1.5 mrad leads to a detuning from the four photon resonance which exceeds the multi-photon linewidth of about 2 MHz. Moreover the Doppler shift which originates from the momentum transfer to the atoms needs to be sufficiently small.

The results of a numerical integration of the Liouville equation [32], using the parameters relevant for the experiment (see below), show the evolution of the population in the various levels, see Figure 2.

Results are shown for laser intensities of 310 mWcm^{-2} corresponding to Rabi- frequency of 0.24 rad/ns, leading to a transfer efficiency of 82%. Increasing the intensity by a factor of 20 will result in a transfer efficiency exceeding 99%. The transient population, which reaches the states $m = +1$ and $m = -1$ in the $^3D_2$ level due to nonadiabatic coupling [2], is negligibly small and will be further reduced when the Rabi frequencies are increased. As much as 30% of the population resides in the $m = 0$ substate of the $^3P_2$ level at intermediate times. Since this level is metastable and there are no processes which interrupt the coherent evolution, all of this population will eventually reach the $m = -2$ final state.

When the laser beams of different polarization propagate in opposite direction, the momentum transfer due to the absorption process (σ^- light) and the stimulated emission process (σ^+ light) occurs in the same direction and the atoms receive a momentum increment of 4 $\hbar k$ transverse to the beam axis. If the atoms return to the initial level, $m = +2$, after passing through a second STIRAP

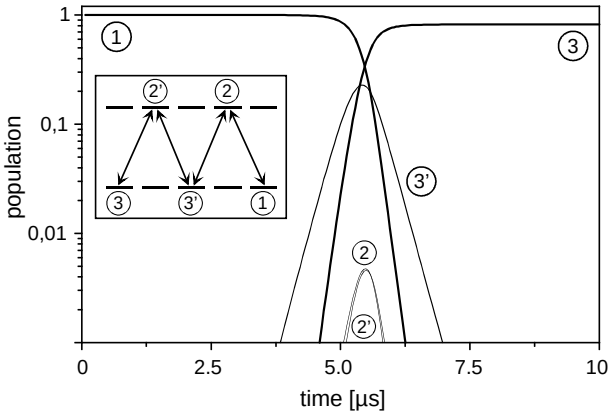

Fig. 2. Evolution of the population in the various m-substates (see Fig. 1) induced by delayed interaction of a Stokes and a pump laser in STIRAP configuration for a laser intensity of 310 mW/cm^2. At this intensity the transfer efficiency is 82%. Increasing the intensity by a factor of 20 would result in a transfer efficiency exceeding 99%. Some transient population resides in level $|3^{'}\rangle$ ($m = 0$). The very small transient population in levels $|2\rangle$ and $|2^{'}\rangle$ ($|m| = 1$ in the $^3D_2$ level) is due to nonadiabatic coupling.

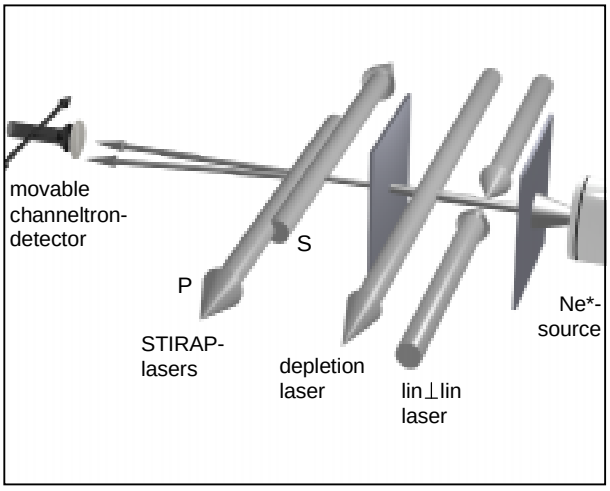

Fig. 3. Setup for the laser aided preparation of the atomic beam. There is an additional aperture, for collimation of the atomic beam, which is not shown. The metastable detection is realized using a channeltron with a slit as entrance aperture mounted on a precision translation stage.

zone a total of 8 $\hbar k$ is transferred, provided the direction of propagation and the sequence of interactions of the σ^- and σ^+ light is interchanged as needed. We note that the discussion of the process in terms of absorption and stimulated emission is illustrative but may be misleading. In the context of STIRAP the stimulated process does not transfer population which resides in the intermediate level to the third level. Rather the transfer occurs through a multi photon process directly from the initially populated level.

3 Experimental

A beam of Ne atoms in metastable states emerges from a cold cathode discharge nozzle source [33–35] which is water cooled, see Figure 3. A fraction of the order of 10^{-4} of the atoms is in the metastable states $^3P_0$ or $^3P_2$ of the $2p^5 3s$ electronic configuration. The flow velocity of the atoms in the beam is about 850 ms^{-1} and the full $1/e^2$-width of the velocity distribution is 300 ms^{-1}. For the experiments discussed in Section 6, the mean longitudinal velocity of the atoms is reduced by cooling the source to liquid nitrogen temperature. Furthermore, divergence of the beam is reduced by one dimensional polarization gradient laser cooling [36] a few cm downstream of the nozzle. For all experiments the population of the $^3P_0$ level of the ^{20}Ne isotope is depleted by optical pumping: A preparation laser (λ =588 nm) excites the atoms to the $^3P_1$ level of the $2p^5 3p$ configuration from where the atoms decay either to one of the metastable levels or to the short lived $^3P_1$ and $^1P_1$ states of the $2p^5 3s$ electronic configuration followed by the emission of an VUV photon (74 nm) as the atoms return to their $^1S_0$ ground state. Since the interaction time of the atoms with the preparation laser is long compared to the lifetime of the upper excited level, all atoms are eventually removed from the metastable $^3P_0$ state.

The beam is collimated by 50 μm and 25 μm wide slits positioned 30 cm and 115 cm, respectively, downstream from the nozzle. These slits provide a collimation of the beam to $1 : 2.3 \times 10^4$. The half $1/e^2$-width of the remaining transvers velocity distribution is equivalent to a photon recoil of 1.2 $\hbar k$. The collimated beam enters the main chamber and intersects the pump and Stokes laser at right angle. The atoms are detected 82 cm further downstream by a channeltron behind a 10 μm slit. Channeltron and slit are mounted on a translation stage, the position of which perpendicular to the atomic beam axis is controlled by a stepper motor with an accuracy of 1 μm.

The earth magnetic field is compensated by three pairs of external coils in Helmholtz arrangement. Flux gate probes [37] measure the components of the magnetic field in all three dimensions near the atomic beam axis with a resolution of 10 nT. Three independent servo loops control the current through the coils. They are used to actively stabilize the magnetic field to any given value and direction. The bandwidth of the servo loop is 1 kHz, which is adequate to compensate time varying homogeneous fields from nearby power supplies.

The laser beam from a Coherent 699 single mode laser, operated with DCM dye, is delivered to the apparatus by a single mode optical fiber. The polarization of the radiation at the fiber exit is controlled by fiber polarizers [38] and a Glan-Thompson prism. The subsequent optical arrangement, which sends this laser beam across the atomic beam with appropriate polarization, direction of propagation and spatial overlap, is shown in Figure 4 for the case when two transfer zones are needed. The beam is reflected by a polarizing beam splitter and circularly polarized by a $\lambda/4$ plate before it crosses the atomic beam at right angle. After passing through a combination of a

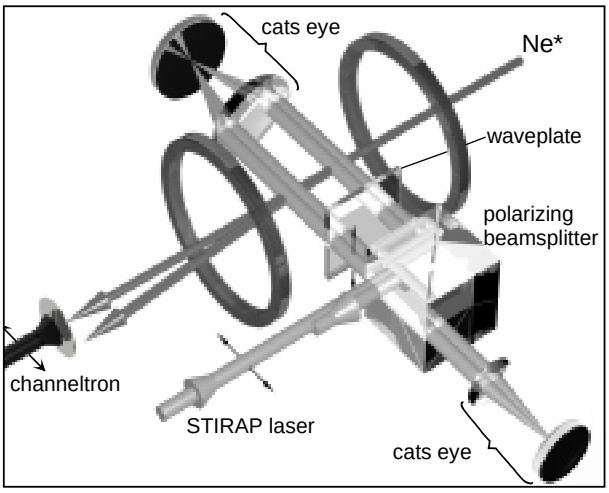

Fig. 4. Optics layout for the dual-zone setup. The combination of lens and mirror acts as a cats eye reflector. The smaller cat eye in the lower part of the figure can be used to control the spatial displacement between both the pump and the Stokes laser while the reflector in the upper part allows to change the distance between the STIRAP zones easily.

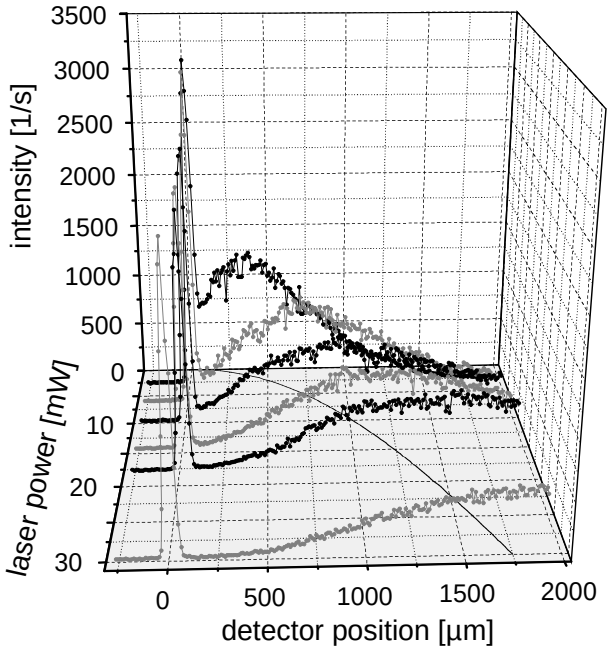

Fig. 5. Atomic beam deflection by the spontaneous emission force, shown here for comparison. The narrow structure is related to the undeflected ^{22}Ne isotope. The beam profile of the deflected ^{20}Ne isotope is shown for the laser powers (3; 6; 10; 15; 18; 30 mW), with the position of the maximum marked in the horizontal plane.

lens and a mirror, equivalent to a cats eye reflector, the laser beam crosses the atomic beam further downstream. It is then linearly polarized again, passes through the polarizing beam splitter and is reflected by a second cats eye arrangement.

The diameter of the laser beams at the crossing with the atomic beam is 3.2 mm ($1/e^2$ full width, measured by a CCD camera). The position of the cats eye arrangements is adjustable parallel to the atomic beam axis. In the setup with two transfer zones, the overlap between the lasers in each of the transfer zones is controlled by one of the cats eye (the smaller one), while the distance between the zones is controlled by the other. The small cats eye needs to be readjusted when the large cats eye is moved. When only one transfer zone is needed only one cats eye is used.

4 Atomic beam deflection

The first successful attempt to deflect particles of an atomic beam by radiation forces dates back as far as 1933 [39]. An example for large angle deflection by spontaneous emission forces, using the same equipment as for the coherent momentum transfer experiment discussed below, is shown in Figure 5. for comparison. Here the coupling is between the levels $^3P_2$ and $^3D_3$ λ =640 nm, which form a closed cycle two level system. The narrow structure is related to the undeflected ^{22}Ne-isotope. The beam profile of the deflected ^{20}Ne-isotope is shown for the laser powers (3; 6; 10; 15; 18; 30 mW), with the position of the maximum marked in the horizontal plane. The location of the maximum increases less than linear with the laser power P. The interaction time is long enough for several hundred absorption emission cycles. Therefore the Doppler shift due to the deflection may be larger than the saturation broadened linewidth. The maximum deflection angle ϑ_{max} is then limited by that linewidth. Since the latter increases proportional to $\sqrt{1+P/P_S}$ [40] where P_S is the saturation power, we have $\vartheta_{max} \sim \sqrt{P}$ for large P. The dependence of spontaneous emission forces on the initial state was recently investigated [41]. Although easy to implement, the dissipative nature of the spontaneous emission process prohibits the use of such an approach when the coherence of the matter waves needs to be maintained.

More recent attempts use, for example, the dipole force exerted on an atom by an evanescent wave, the frequency of which was detuned far to the blue side of the transition frequency (see *e.g.* [42–44]). The application of two π-pulses from counterpropagating beams is a common approach [45–47] in Ramsey-type atomic interferometry [48]. In the former approach relatively high laser power is needed, while in the latter one radiative loss from the intermediate state may be a problem. Alternative schemes using magnetic forces have also been discussed recently [49].

It is a distinct advantage of coherent momentum transfer by the STIRAP process, that the dissipative process of spontaneous emission is eliminated, even when short lived intermediate states are used [50]. Furthermore, because of the resonant coupling of the atomic levels moderate power, within the limits imposed by the adiabatic following condition [2], is adequate. Finally, since the STIRAP process evolves along a zero energy eigenstate, the consequences

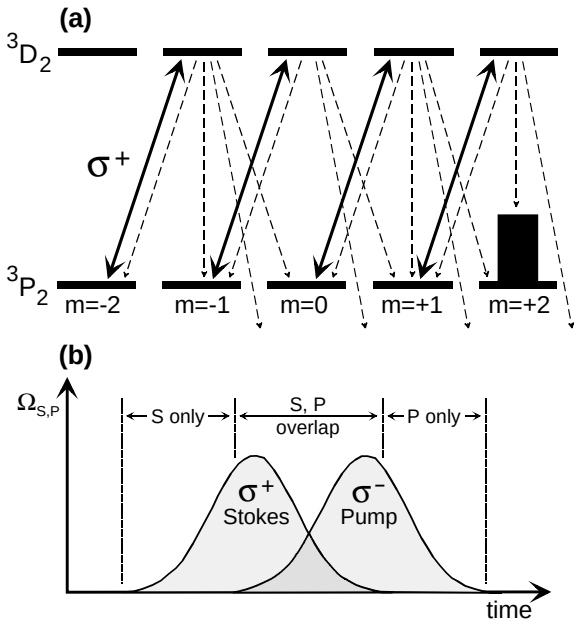

Fig. 6. The interaction sequence of circularly polarized light in the STIRAP configuration, shown in the lower part, prepares the atoms automatically in the $m = +2$ substate, see upper part of the figure.

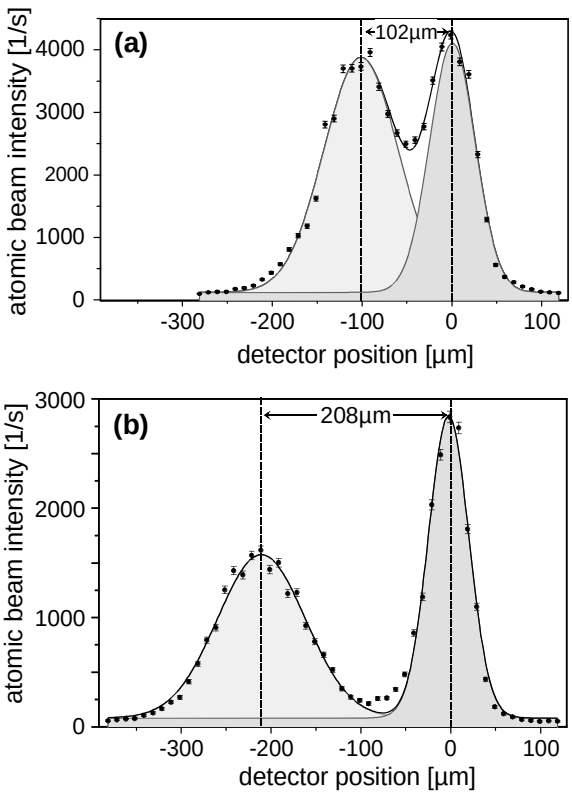

Fig. 7. Profile of the beam of ^{20}Ne atoms with respect to the ^{22}Ne isotope (the latter marks the position and profile of the original beam) with a single transfer zone (a) and a dual transfer zone arrangement (b). In the former case a total momentum of 4 $\hbar k$ is coherently transferred while the transfer is 8 $\hbar k$ in the latter case. The maximum of the deflected beam (b) is not exactly twice the displacement seen in (a) because of some incoherent momentum transfer due to the Stokes laser induced optical pumping, see Figure 6. The longitudinal velocity distribution is the main cause for the broadening of the profile of the deflected beam with respect to the undeflected one. The deflection angle related to the maximum in (b) is 0.25 mrad.

of an AC Stark shift of the phase of the matter wave, and the sensitivity of an interferometric setup to a small variation of the laser power, is reduced or even eliminated.

In the present experiment, we transfer atoms back and forth between magnetic substates with $|m| = 2$. Such a process has been demonstrated before in the time domain [51]. There is no need to prepare the atoms initially in the $m = +2$ *via* optical pumping by a separate laser before they reach the transfer zones because this preparation is intrinsic. The atoms are initially exposed to the σ^+ radiation. The population of all levels other than $m = +2$ is depleted by optical pumping provided the atoms are exposed to the Stokes laser radiation long enough to undergo several optical pumping cycles before they reach the region where the two laser beams overlap, see Figure 6. The lifetime of the $^3D_2$ state is 19.6 ns [52]. Therefore the extension of the zone with only the Stokes laser present, should be (for particles traveling at a speed of the order of 1000 m/s) no less than 0.1 mm. In our experiment, it is about 1 mm wide.

The profile of the atomic beam is detected by a channeltron behind a 10 μm slit 82 cm downstream of the transfer zone. An example with only one transfer zone in place is shown in Figure 7a, while the profile determined by the accumulated deflection of two transfer zones is given in Figure 7b. The ^{22}Ne atoms do not interact with the radiation field. They are detected on axis. The width of the peak is determined by the collimation of the atomic beam. As shown in Figure 7b the profile of the deflected beam is fully separated from the primary beam.

Due to the longitudinal velocity distribution of atoms in the beam the width of the deflected beam is broader than that of the undeflected one. Comparison of the data shown in Figures 7a and b reveals that the displacement due to a momentum transfer of 4 $\hbar k$ is 106 μm. The exact position of the maximum of the distribution and the increase in width are determined by two contributions:

(i) Some population reaches the $m = +2$ state during the flight-path through the wings of the Stokes laser beam profile after having absorbed and reemitted at least one photon. Numerical simulation shows that this initial optical pumping process leads, at the average, to a shift of the distribution by 5 μm in the direction of propagation of the Stokes laser, *i.e.* in the opposite direction compared to the deflection by the coherent moment transfer. This explains why the maximum of the peak after the transfer of 4 $\hbar k$ is found at a position

less than half of the displacement found for the 8 $\hbar k$ peak.

(*ii*) The momentum transfer perpendicular to the atomic beam axis is (except for the small contribution from the incoherent process discussed under (*i*)) precisely 8 $\hbar k$. The momentum distribution parallel to the atomic beam axis is, however, determined by the velocity distribution of the atoms. A time-of-flight analysis of the deflected atoms would show a peak the width of which is similar to the one of the undeflected ^{22}Ne atoms while its angular position would change with the flight time (*i.e.* with the velocity parallel to the beam axis).

Comparison of the area of the deflected and undeflected beams allows the calibration of the efficiency of the transfer. The natural abundance of the ^{22}Ne isotope is 9.5%. Assuming uniform population of the m-substates of the $^3P_2$ level, 20% of the atoms in that state are in the $m = +2$ state. From the branching ratios in the optical pumping processes we find the ratio of the area of the deflected and undeflected beam should be $\gamma = 2.02 : 1$ for a transfer efficiency of unity[1]. A background count rate of about 100 s^{-1} (indicated by the thin line in Fig. 7) needs to be subtracted from the signals. It results from the emission of VUV photons from the nozzle. This radiation is diffracted by the 25 μm collimating slit. The zero order maximum of the diffracted light has a width of 2.8 mm at the plane of the detector and contributes to a background signal which is nearly constant over the relevant area shown. After correction for this background signal the ratio of peak areas is $\gamma = (1.54 \pm 0.06) : 1$ which corresponds to a reflectivity of a single transfer zone of $R = (76 \pm 3)\%$, in good agreement with the results shown in Figure 2. Simulations show that a power density of 6 W/cm^2 (rather than 0.3 W/cm^2 used when the data of Fig. 7 was recorded) would yield a reflectivity exceeding 99%, provided the increase in laser power is not accompanied by detrimental influences such as induced by stray light.

We emphasize that the deflection angle related to coherent momentum transfer is, in contrast to the data shown in Figure 5, independent of the laser power, provided that adiabaticity [2] is satisfied. This is shown in Figure 8. For small laser power (< 2 mW) the efficiency of the atomic beam deflector is rather small because in this case the adiabaticity criterion is not fulfilled. Some population reaches the intermediate states in the $^3D_2$ level from which the atoms decay to the ground state. For higher laser power (> 30 mW) the adiabaticity criterion is satisfied. We observe, however, a decreasing transfer efficiency with increasing power. In fact, stray light from the windows, which does not affect the undeflected beam of ^{22}Ne atoms and possibly optical pumping induced by imperfect polarizations of the laserbeams reduce the population of atoms in the $^3P_2$ states of ^{20}Ne.

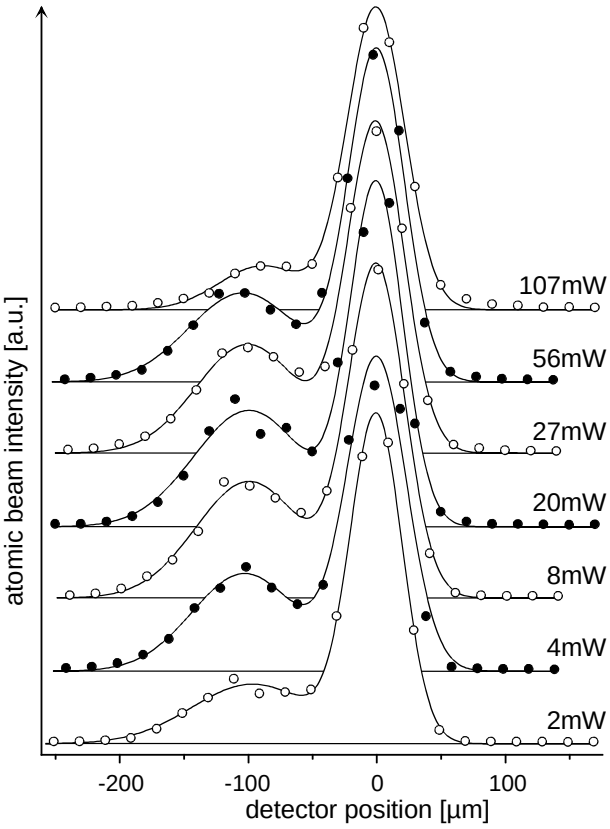

Fig. 8. Atomic beam deflection by a single STIRAP zone as a function of the laser power. The structure on the left is related to the deflected atoms in the $^3P_2$ state. This data was measured without depopulating the $^3P_0$ state. Therefore the reference peak is more intense compared to Figure 7a.

Finally, we show in Figure 9 the typical signature of the STIRAP process for a power of the laser beam of 25 mW. The gray-scale representation shows the intensity of the deflected and the undeflected beam as the spatial overlap of the pump and Stokes lasers is changed. The vertical scale gives the displacement ϵ of the axis of the laser beams in units of the diameter d of the beams. The zero of the vertical axis is precisely determined by observing, at the entrance side of the fiber, the reflected intensity which is coupled back into it. The axis of the σ^+- and σ^-- beam coincide, when this intensity is maximal. The data of Figure 9 confirmes that the efficiency of the

[1] A fraction of 1/6 and 5/6 of the atoms is found in the $^3P_0$ and $^3P_2$ metastable states, respectively. Assuming uniform distribution of the population over m-states, we have 16.7% of the ^{20}Ne atoms in the $m = +2$ state of the $^3P_2$ level. Based on the relevant branching ratios we find that optical pumping transfers 4% of the $^3P_0$ level to the $m = +2$ state of the $^3P_2$ level adding 0.67% with respect to the initial population of ^{20}Ne in metastable levels. Furthermore, transfer by optical pumping from the $m = +1$ state of $^3P_2$ adds another 3.89% to the population of that state. Therefore the $m = +2$ state of $^3P_2$ carries 21.26% of the population of ^{20}Ne atoms initially in a metastable state when they reach the overlap region of the (first) STIRAP zone. With the natural abundance of 90.5% for ^{20}Ne, we therefore find 19.24% of all metastable atoms in the $^3P_2$ ($m = +2$) state, which is a factor of 2.02 more than the 9.5% natural abundance of the ^{22}Ne isotope.

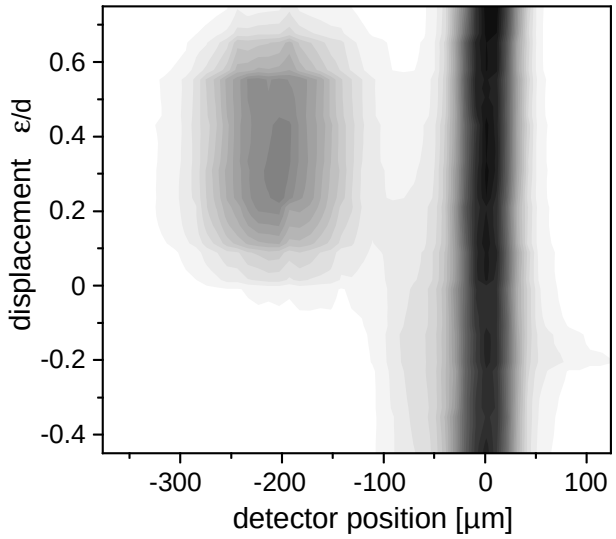

Fig. 9. The "STIRAP-signature" of coherent momentum transfer. Large deflection angles are observed when the laser beams are spatially shifted. The deflection signal shown is observed when the interaction of the atoms is first with the Stokes (corresponding to positive values of ϵ/d). Since the m-state preparation is intrinsic an equivalent deflection signal (not shown) is observed around $\epsilon/d \approx -0.4$ and a detector position near $+200$ μm.

momentum transfer is insensitive to small variations of the spatial overlap of the pump- and Stokes laser. This is another example demonstrating the remarkable robustness of the STIRAP process [2].

5 Dependence on weak magnetic fields

Methods for measuring small magnetic fields are well established. These include traditional devices such as flux gate or Hall effect sensors [37] and very sensitive optical pumping schemes [53,54]. New methods based on the highly dispersive nature of coherently coupled quantum states [55–57], are emerging as well. It has also been shown that the interplay of the Larmor precession and the momentum transfer which accompanies optical pumping in a closed loop system renders the deflection of a beam of metastable He atoms sensitive to a magnetic field in the region where optical pumping occurs. Implementation of this "mechanical Hanle effect" [58] requires a closed loop level system with $j_u \leq j_l$ ($j_l \neq 0$) where u and l refer to the upper and lower level respectively in the two level system. Such a closed loop level system is not available for Ne*.

Here we demonstrate how the interplay of the Larmor precession and the deflection by coherent momentum transfer can be used to measure the magnetic field along the axis of the molecular beam, averaged over the flight-path given by the distance between the two STIRAP deflection zones. Such an *in situ* measurement of the magnetic field, often needed to zero it, is required for many atom optics experiments.

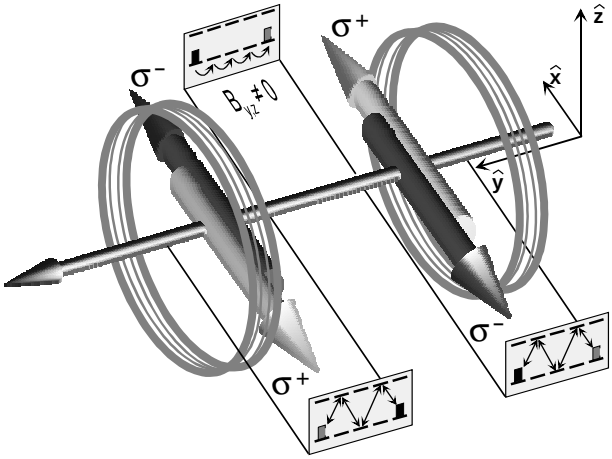

Fig. 10. This figure shows the interaction region (the central part of Fig. 4) for the Larmor velocity filter in combination with the transfer of population between m-states which takes place either in the two STIRAP zones or in the flight path between both zones induced by the magnetic field.

Consider the dual-zone arrangement, shown in Figure 10. In the first zone, atoms are prepared in the $m = +2$ substate and transferred to $m = -2$. They will be transferred back to the initial quantum state in the second zone, provided they remain in the $m = -2$ state along the flight-path between the two zones. When the laser beams are counterpropagating, as shown in the figure, the momentum transfer of 8 $\hbar k$ results in the deflection, see Figure 7b. The intensity at the maximum of the profile of the deflected beam is proportional to the flux of atoms in the $m = -2$ magnetic substate at the location of the second transfer zone. Larmor precession due to a magnetic field in the region between the two transfer zones will therefore interfere with the momentum transfer. In fact, a nonvanishing component of the magnetic field perpendicular to this initial quantization axis will result in a Larmor precession and the m-states will be mixed during their flight between the zones. The Larmor precession angle evolves as

$$\Theta = \bar{\omega}_{Larmor}\, t_{flight} \tag{5.1}$$

with $t_{flight} = D/v$, where D is the distance between the transfer zones, v is the velocity of the atoms along the atomic beam axis taken as the y-direction, and the flight-path averaged Larmor frequency

$$\bar{\omega}_{Larmor} = \frac{g_J \mu_B}{\hbar} \bar{B} \tag{5.2}$$

with

$$\bar{B} = \frac{1}{D} \int_0^D \sqrt{B_y^2(y) + B_z^2(y)}\, dy\,. \tag{5.3}$$

The fraction of atoms found in the state $|m^{'}\rangle = |-2\rangle$ at the second transfer zone is determined as follows: After the first deflection zone the atoms are found in the state $|m^{'}\rangle = |-2\rangle$ by transfer from the initially prepared quantum state $|+2\rangle$. A maximum of the flux of deflected atoms will be observed when the Larmor precession angle Θ along the flight-path to the second transfer zone is $\Theta = n\pi$, *i.e.* when all of the population of the magnetic substate $|m^{'}\rangle$, which is coupled by the magnetic interaction to other substates has returned to the substate $|m^{'}\rangle$. The variation of the flux of deflected atoms with $\bar{B}$ is discussed next.

The projection of the substate $m^{'}$ at time $t = 0$, $|m^{'}, 0\rangle$, referring to the quantization axis parallel to $\hat{k}$, onto the substates $|M^{'}, 0\rangle$ defined with respect to the quantization axis $\hat{B}$ with the angle $\beta = \angle(\hat{B}; \hat{k})$, is $\langle m^{'}, 0|M^{'}, 0\rangle = d^{(2)}_{m^{'},M^{'}}(\beta)$ where $d^{(2)}_{m^{'},M^{'}}(\beta)$ is the reduced rotation matrix element for $J = 2$. The state vector $|M^{'}; t, \bar{B}\rangle$ evolves according to

$$|M^{'}; t, \bar{B}\rangle = d^{(2)}_{m^{'},M^{'}}(\beta)|m^{'}, 0\rangle \exp\left(-i\Theta(t, \bar{B})M^{'}\right). \quad (5.4)$$

The projection of the states $|M^{'}; t, \bar{B}\rangle$ on the quantization axis defined by $\hat{k}$ results in the vector $|m^{''}; t, \bar{B}\rangle$ given by

$$|m^{''}; t, \bar{B}\rangle = \sum_{M^{'}} d^{(2)}_{M^{'},m^{''}}(-\beta)|M^{'}; t, \bar{B}\rangle. \quad (5.5)$$

For $t = t_{flight}$ this reads

$$|m^{''}; t_{flight}, \bar{B}\rangle = \left[\sum_{M^{'}} d^{(2)}_{m^{'},M^{'}}(+\beta) d^{(2)}_{M^{'},m^{''}}(-\beta) \times \exp\left(-i\Theta(t_{flight}, \bar{B})M^{'}\right)\right] |m^{'}, 0\rangle . \quad (5.6)$$

Population in state $|m^{'}\rangle$ at $t = 0$ which is found later in state $|m^{''}\rangle$ at $t = t_{flight}$ is given by

$$P_{m^{''},m^{'}}(t_{flight}, \bar{B}) = \left[\sum_{M^{'}} d^{(2)}_{m^{'},M^{'}}(+\beta) d^{(2)}_{M^{'},m^{''}}(-\beta) \times \exp\left(-i\Theta(t_{flight}, \bar{B})M^{'}\right)\right]^2 . \quad (5.7)$$

Applied to our experimental situation $\beta = \pi/2$ and $m^{'} = m^{''} = -2$ equation (5.7) yields

$$P_{-2,-2}(t_{flight}, \bar{B}) = \frac{1}{64}\left[\cos 2\Theta(t_{flight}, \bar{B}) + 4\cos\Theta(t_{flight}, \bar{B}) + 3\right]^2 \quad (5.8)$$

or, using trigonometrical identities and the definition of $\Theta(t_{flight}, \bar{B})$ (Eqs. (5.1) and (5.2)):

$$P_{-2,-2}(t_{flight}, \bar{B}) = \left(\cos\frac{\mu_B g_J}{2\hbar} t_{flight}\bar{B}\right)^8 . \quad (5.9)$$

Only the atoms in the substate $m = -2$ will acquire an additional momentum of $4\,\hbar k$. Atoms in other states are excited to the $^3D_2$ state by the first radiation field of the second transfer zone from where most of them decay to the ground state and therefore do not reach the detector. For completeness we also give the probabilities for finding atoms in magnetic substates other than $m = -2$:

$$P_{-1,-2}(t_{flight}, \bar{B}) = 4\left(\cos\frac{\mu_B g_J}{2\hbar} t_{flight}\bar{B}\right)^6 \times \left(\sin\frac{\mu_B g_J}{2\hbar} t_{flight}\bar{B}\right)^2$$

$$P_{0,-2}(t_{flight}, \bar{B}) = 6\left(\cos\frac{\mu_B g_J}{2\hbar} t_{flight}\bar{B}\right)^4 \times \left(\sin\frac{\mu_B g_J}{2\hbar} t_{flight}\bar{B}\right)^4$$

$$P_{+1,-2}(t_{flight}, \bar{B}) = 4\left(\cos\frac{\mu_B g_J}{2\hbar} t_{flight}\bar{B}\right)^2 \times \left(\sin\frac{\mu_B g_J}{2\hbar} t_{flight}\bar{B}\right)^6$$

$$P_{+2,-2}(t_{flight}, \bar{B}) = \left(\sin\frac{\mu_B g_J}{2\hbar} t_{flight}\bar{B}\right)^8 .$$

Equation (5.9) reveals that $P_{-2,-2}(t_{flight}, \bar{B})$ is very sensitive to the **B**-field for

$$\Theta(t_{flight}, \bar{B}) = n\pi, \qquad n = 0, 1, 2, ... \quad (5.10)$$

Upon increasing of the magnetic field strength a periodic change of the detector signal will be observed, reaching a maximum value when the condition equation (5.10) is fulfilled.

According to equation (5.9), we can expect a very narrow central maximum ($n = 0$), but broader structures for $n > 0$ since the precession angle depends on the velocity. The velocity dependence of $\Theta(t_{flight}, \bar{B})$ will be used to design a "Larmor velocity filter", see Section 6.

Figure 11 shows experimental results together with those from simulation studies. The magnetic field in the z-direction is scanned *via* electronic control of the current through the Helmholtz coils while the field in the y-direction is varied in increments. Since the field strengths which leads to $\Theta(t_{flight}, \bar{B}) = n\pi$ depends on the direction of the field perpendicular to the direction of the laser beam but is independent of the azimuthal angle, a circular structure is seen. The results for a flight-path of 2.5 mm or 5.5 mm, shown in Figure 11a or b, reveal the $n = 0$ and $n = 1$ or the $n = 0, 1, 2$ and 3 maxima, respectively, in agreement with the results from the simulation studies, Figure 11c and d.

The consequences of the velocity dependence of the Larmor precession angle accumulated during the flight-path between the transfer zones is more clearly recognizable in Figure 12, which shows results from a different set of experiments with enhanced on-axis intensity, achieved by one-dimensional polarization gradient cooling. The data shown in this figure correspond to a cut through data, such as shown in Figure 11, for $B_y = 0$.

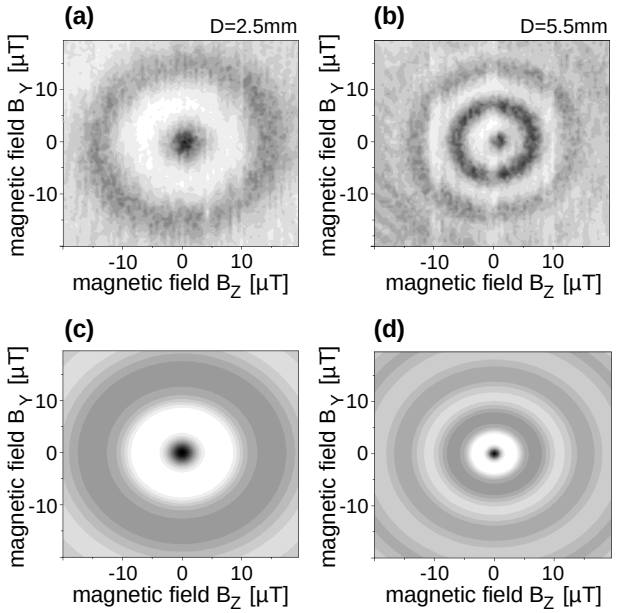

Fig. 11. Variation of the atomic beam intensity at the position of the maximum of the deflected beam (dual zone arrangement) as a function of the magnetic field in z- and y-direction. Dark areas indicate high intensity. Deflection by coherent momentum transfer of 8 $\hbar k$ is only possible for zero magnetic field or for a field which allows n full Larmor precession cycles. Since the Larmor frequency depends only on the magnitude of the component of the magnetic field perpendicular to the quantization axis, a circular structure is seen. The panels (a) and (b) show experimental results for a separation of the transfer zone by 2.5 mm and 5.5 mm respectively. Related results of simulation studies are shown in panels (c) and (d).

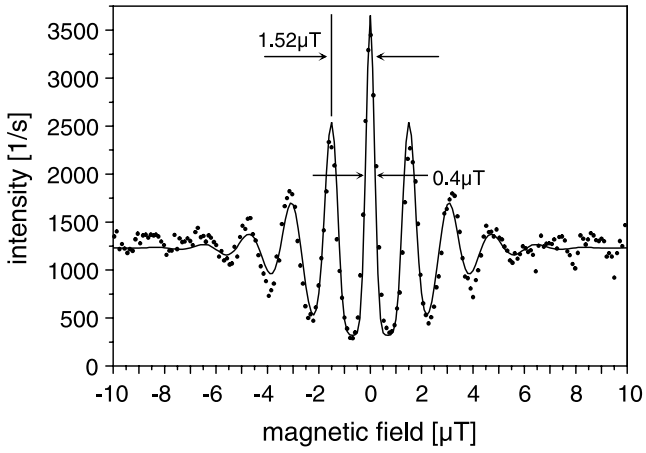

Fig. 12. The interplay of Larmor precession and deflection by coherent momentum transfer in the dual zone arrangement as B_x is varied for $B_y = 0$ together with simulation studies based on equation (5.9) including the longitudinal velocity distribution of the atoms in the beam. The spatial separation of the two STIRAP zones is 23 mm.

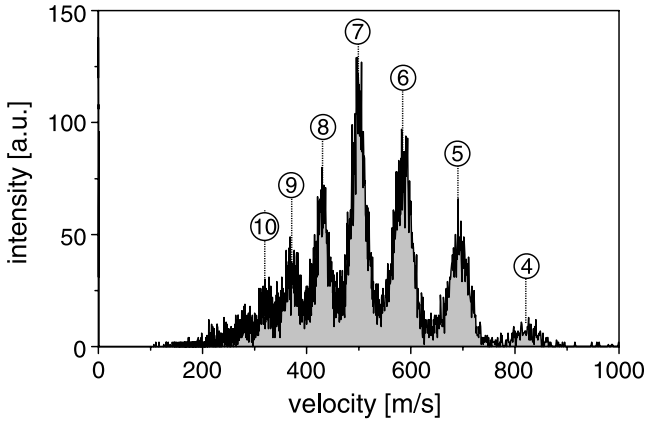

Fig. 13. Time-of-flight spectra for the dual zone coherent momentum transfer arrangement for $B = 20$ μT.

Obviously, the maximum intensity at the peaks is reduced as they broaden with increasing order n. The intensity near the central peak falls to 50% of its maximum value at a magnetic field of about $B = 0.4$ μT. This value determines the precision with which the magnetic field can be nulled by the external coils in the present experimental arrangement. We are in the process of installing a Zeeman slower to reduce the atomic beam velocity. Reduction of the velocity of the atoms to 100 m/s will increase the sensitivity to 100 nT (or 1 mG). Increasing the length of the flight-path between the transfer zones would further increase the sensitivity. An accuracy of the order of 10 nT over a 50 mm long flight path should be achievable.

6 The Larmor velocity filter

The velocity dependence of the precession angle, equation (5.9), is demonstrated in Figure 13. The discharge source is pulsed for time-of-flight analysis. The typical length of the pulses was 10 μs.

The distribution of arrival times at the position of the deflected beam is converted to a distribution of velocities. The magnetic field perpendicular to the quantization axis is set at 20 μT, which is far beyond the value that allows the resolution of individual peaks in Figure 12. The number above the peaks in Figure 13 give the number n of full Larmor precession cycles during the flight time between the two transfer zones. We have $n = 4$ for $v \approx 840$ m s^{-1}, $n = 7$ for $v \approx 500$ m s^{-1} and $n = 10$ for $v \approx 320$ m s^{-1}. The envelop of the peaks reflects the velocity distribution for the atoms in the beam. Clearly, only atoms with a certain velocity are transmitted through this "Larmor velocity filter" arrangement.

Once the order n of the maxima, such as those seen in Figure 13, is known and the corresponding velocity v_{max} is measured, the strength of the B-field in the direction perpendicular to the laser beams can be determined. Reducing the B-field results in a reduction of the v_{max}. A "Larmor velocity filter" can also be implemented with

copropagating pump and Stokes laser in the two transfer zones. The net momentum transfer will be zero in such an arrangement and the velocity distribution of the atoms, transmitted through the two STIRAP zones can be determined at the atomic beam axis. Atoms at velocities, which fulfill the resonance condition between the flight time from one transfer zone to the other (*i.e.* execute n cycles of the Larmor precession), will be transmitted and recorded at the detector. All other atoms will be lost from the metastable state by optical pumping.

7 Conclusion

We have demonstrated experimentally that efficient coherent momentum transfer by partially overlapping laser pulses can be used to fully separate the deflected and undeflected part of the atomic beam. The process makes use of the same concept as the STIRAP technique, which was developed for population transfer. The interaction, which leads to the deflection, is nondissipative. Although some energy due to the photon recoil is added to the particle, this element can be used in atom optics experiment, in particular in the context of interferometry, since coherence is preserved. The reflectivity of the mirror, discussed in this paper, is of the order of 80%. However, increase in laser power will increase the reflectivity to values much closer to unity. We have shown deflection by up to two sequential transfer zones. Adding more of such zones will allow larger deflection angles. It was furthermore shown, how the effect of the Larmor precession during the flight-path between transfer zones can be used to determine the magnetic field perpendicular to the laser beam propagation. In particular, external control of the current through the Helmholtz coils may lead to the desired cancellation of the field, a process which can be monitored with the help of the Larmor velocity filter. With atoms slowed to 100 $\mathrm{m\,s^{-1}}$ an accuracy, integrated over the flight-path between the transfer zones, of the order of 10 nT (0.1 mG) is achievable, corresponding to a Larmor frequency (for electrons in the quantum state use in this experiment) of the order of 100 Hz.

We thank Dr. Razmik Unanyan (Armenian Academy of Sciences, Ashtarak), Dr. B.W. Shore (Lawrence Livermore National Laboratory) and Prof. Yuzhu Wang (Shanghai Institute of Optics and Fine Mechnics, SIOFM) for fruitful discussion and L. Yatsenko for carefully reading the manuscript. K.B. also thanks the Max-Planck Gesellschaft and the Chinese Academy of Science for supporting a visit to the SIOFM, during which some of the ideas which lead to this work were developed. Financial support by the Deutsche Forschungsgemeinschaft and partial support by the EU (HCM network ERB-CHR-XCT-94-0603) is acknowledged. We thank Katrin Klein and Christa Habscheid for their help in the experiments of Section 6.

References

1. J. Oreg, F.T. Hioe, J.H. Eberly, Phys. Rev. A **29**, 690 (1984).
2. U. Ganbatz, P. Rudecki, S. Schiemann, K. Bergmann, J. Chem. Phys. **92**, 5363 (1990).
3. S. Schiemann, A. Kuhn, S. Steuerwald, K. Bergmann, Phys. Rev. Lett. **71**, 3637 (1993).
4. T. Halfmann, K. Bergmann, J. Chem. Phys. **104**, 7068 (1996).
5. J. Martin, B.W. Shore, K. Bergmann, Phys. Rev. A **54**, 1556 (1996).
6. S.E. Harris, Phys. Today 36 (1997).
7. G. Alzetta, A. Gozzini, L. Moi, G. Orriols, Nuovo Cimento B **36**, 5 (1976).
8. E. Arimondo, G. Orriols, Nuovo Cimento **17**, 333 (1976).
9. E. Arimondo, Phys. Rev. A **54**, 2216 (1996).
10. B.W. Shore, *The Theory of Coherent Atomic Excitation* (John Wiley & sons, New York, 1990).
11. K. Bergmann, H. Theuer, B.W. Shore, Rev. Mod. Phys. **70** (July, 1998).
12. P. Dittmann, F.P. Pesl, J. Martin, G. W. Coulston, G.Z. He, K. Bergmann, J. Chem. Phys. **97**, 9472 (1992).
13. M. Külz, M. Keil, A. Kortyna, B. Schellhaaß, J. Hauck, K. Bergmann, Phys. Rev. A **53**, 3324 (1996).
14. R. Sussmann, R. Neuhauser, H.J. Neusser, J. Chem. Phys. **100**, 4784 (1994).
15. R. Sussmann, R. Neuhauser, H.J. Neusser, J. Chem. Phys. **103**, 3315 (1995).
16. S. Kulin, B. Saubamea, E. Peik, J. Lawall, T.W. Hijmans, M. Leduc, C. Cohen-Tannoudji, Phys. Rev. Lett. **78**, 4185 (1997).
17. W. Süptitz, B.C. Duncan, P.L. Gould, J. Opt. Soc. Am. B **14**, 1001 (1997).
18. L.S. Goldner, C. Gerz, R.J.C. Spreeuw, S.L. Rolston, C.I. Westbrook, W.D. Phillips, Phys. Rev. Lett. **72**, 997 (1994).
19. M. Weitz, B.C. Young, S. Chu, Phys. Rev. Lett. **73**, 2563 (1994).
20. M. Weitz, T. Heupel, T.W. Hänsch, Phys. Rev. Lett. **77**, 2356 (1996).
21. P.D. Featonby, G.S. Summy, J.L. Martin, H. Wu, K.P. Zetie, C.J. Foot, K. Burnett, Phys. Rev. A **53**, 373 (1996).
22. R. Walser, J.I. Cirac, P. Zoller, Phys. Rev. Lett. **77**, 2658 (1996).
23. B. Nölle, H. Nölle, J. Schmand, H.J. Andrä, Europhys. Lett. **33**, 261 (1996).
24. J. Söding, R. Grimm, Yu. B. Ovchinnikov, Ph. Bouyer, Ch. Salomon, Phys. Rev. Lett. **78**, 1420 (1997).
25. A. Goepfert, I. Bloch, D. Haubrich, F. Lison, R. Schütze, R. Wynands, D. Meschede, Phys. Rev. A **56**, R 3354 (1997).
26. J. Lawall, M. Prentiss, Phys. Rev. Lett. **72**, 993 (1994).
27. B.W. Shore, K. Bergmann, J. Oreg, S. Rosenwaks, Phys. Rev. A **44**, 7442 (1991).
28. P. Pillet, C. Valentin, R.-L. Yuan, J. Yu, Phys. Rev. A **48**, 845 (1993).
29. D.S. Weiss, B.C. Young, S. Chu, Appl. Phys. B **59**, 217 (1994).
30. J. Martin, B.W. Shore, K. Bergmann, Phys. Rev. A **52**, 583 (1995).
31. K. Bergmann, B.W. Shore, in *Molecular Dynamics and Spectroscopy by Stimulated Emission Pumping*, edited by H.L. Dai, R.W. Field (World Scientific, Singapore, 1995).

32. B.W. Shore, J. Martin, M.P. Fewell, K. Bergmann, Phys. Rev. A **52**, 566 (1995).
33. W. Bußert, T. Bregel, R.J. Allan, M.W. Ruf, H. Hotop, Z. Phys. A **320**, 105 (1985).
34. S. Schohl, D. Klar, T. Kraft, H.A.J. Meijer, M.W. Ruf, U. Schmitz, S.J. Smith, H. Hotop, Zeitschrift für Physik D – Atoms Molecules and Clusters **21**, 25 (1991).
35. R. Kau, I.D. Petrov, V.L. Sukhorukov, H. Hotop, J. Phys. B **29**, 5673 (1996).
36. H. Metcalf, P. van der Straten, Phys. Reports **244**, 203 (1994).
37. R. Boll, K.J. Overshold, *Magnetic Sensors*, edited by W. Göpel, J. Hesse and J. N. Zemel (VCH, Weinheim, 1989).
38. H.C. Lefevre, Electronic Lett. **16**, 778 (1980).
39. R. Frisch, Z. Phys. **86**, 42 (1933).
40. W. Demtröder, *Laserspektroskopie*, 2nd edition (Springer Verlag, Berlin Heidelberg New York, 1991) p. 286.
41. G.S. Summy, B.T.H. Varcoe, W.R. MacGillivray, M.C. Standage, J. Phys. B **30**, L541 (1997).
42. R.J. Cook, R.K. Hill, Optics Communications **43**, 258 (1982).
43. V.I. Balykin, V.S. Letokhov, Yu. B. Ovchinnikov,A.I. Sidorov, JETP Lett. **45**, 282 (1987).
44. W. Seifert, C.S. Adams, V.I. Balykin, C. Heine, Y. Ovchinnikov, J. Mlynek, Phys. Rev. A **49**, 3814 (1994).
45. M. Kasevich, D.S. Weiss, E. Riis, K. Moler, S. Kasapi, S. Chu, Phys. Rev. Lett. **66**, 2297 (1991).
46. F. Riehle, A. Witte, T. Kisters, J. Helmcke, Appl. Phys. B **54**, 333 (1992).
47. U. Sterr, K. Sengstock, J.H. Müller, D. Bettermann, W. Ertmer, Appl. Phys. B **54**, 341 (1992).
48. P.R. Berman, *Atom Interferometry* (Academic Press, San Diego, 1997).
49. W.G. Kaenders, F. Lison, I. Müller, A. Richter, R. Wynands, D. Meschede, Phys. Rev. A **54**, 5067 (1996).
50. P. Marte, P. Zoller, J.L. Hall, Phys. Rev. A **44**, 4118 (1991).
51. M. Weitz, B.C. Young, S. Chu, Phys. Rev. Lett. **73**, 2563 (1994).
52. P. Hartmetz, H. Schmoranzer, Z. Phys. A - Atoms and Nuclei **317**, 1 (1984).
53. C. Cohen-Tannoudji, J. DuPont-Roc, S. Haroche, F. Laloë, Phys. Rev. Lett. **22**, 758 (1969).
54. M.D. Hooglerland, J.P.D. Driesen, E.J.D. Vredenbregt, H.J.L. Megens, M.P. Schuwer, H.C.W. Beijerinck, and K.A.H. van Leeuwen, Europhys. Lett. **19**, 669 (1992).
55. M.O. Scully, Phys. Rev. Lett. **67**, 1855 (1991).
56. M.O. Scully, M. Fleischhauer, Phys. Rev. Lett. **69**, 1360 (1992).
57. A.S. Zibrov, M.D. Lukin, L. Hollberg, D.E. Nikonov, M.O. Scully, H.G. Robinson, V.L. Velichansky, Phys. Rev. Lett. **76**, 3935 (1996).
58. R. Kaiser, N. Vansteenkiste, A. Aspect, E. Arimondo, C. Cohen-Tannoudji, Z. Phys. D **18**, 17 (1991).